Higgs Boson: Spin and CP

Katharina Schleicher*

Physikalisches Institut
Universität Freiburg
Hermann-Herder-Str. 3, 79104 Freiburg, Germany

September 6, 2014

Abstract

After the discovery of a new boson in July 2012 at CERN it got important to investigate its properties. That implies the study of its spin- and CP-nature. This paper summarises the analyses in three channels by ATLAS and CMS. The presented channels are $H \to \gamma\gamma$ (just spin-analysis), $H \to ZZ^* \to 4\ell$ and $H \to WW^* \to e\nu_e\mu\nu_\mu$ (just ATLAS). Moreover the combination of the results of the three channels by ATLAS is introduced. The standard model prediction $J^P = 0^+$ and several alternative models with spin=0, spin=1, spin=2 and CP-even or -odd are tested. Furthermore the influence on the sensitivity due to two different production modes for one of the spin-2 models is analysed.

*katharina.schleicher@mars.uni-freiburg.de

1 Introduction

There was the discovery of a new boson in July 2012. After investigating some of its properties like coupling strengths which are compatible with the standard model (SM) more properties like spin and CP have to be tested. For this purpose the SM-hypothesis for spin ($J = 0$) and CP (+) is compared to other hypotheses depending on certain models. In this paper the analyses in three different channels by ATLAS and CMS are presented.

The structure of this paper is as follows. First there is a short theory part. Afterwards the analyses in three different channels are presented. It is started with the main part, the channel $H \to \gamma\gamma$ by ATLAS in more detail, followed by a short comparison with the results by CMS, section 3. Afterwards the analysis in the channel $H \to ZZ^* \to 4\ell$ by CMS with a brief comparison with ATLAS is shown, section 4. Then the analysis by ATLAS of the third channel $H \to WW^* \to e\nu_e\mu\nu_\mu$ is presented, section 5, followed by the combination of the three channels for the analyses by ATLAS, section 6. In the end of section 3 and 6 the influence by two different production modes for one of the spin-2 models on the sensitivity is analysed shortly.

2 Theory

Since the Higgs-Field is a scalar field also the SM-Higgs-Boson is assumed to be a scalar particle, i.e. spin $J = 0$.

Because of the observation of the decay $H \to \gamma\gamma$ the case spin $J = 1$ is ruled out by the Landau-Yang theorem which says that a massive spin-1 particle cannot decay into a pair of identical massless spin-1 particles (e.g. two photons).

A spin-2 particle would not be compatible with a renormalizable theory.

The spin-nature of a particle can be investigated through the longitudinal spin-correlations of its decay particles.

The CP-nature of the SM-Higgs-Boson is CP-even (+) and hence it is an eigenstate to the CP-operator. There are two eigenvalues, $+1$ and -1. The letter C stands for charge-conjugation (exchange of particle by its antiparticle) and the letter P for parity (mirroring of all space coordinates). Thus a system is CP-symmetric if nothing changes if the particles are replaced by their antiparticles and simultaneously all space coordinates are mirrored. If the Higgs-Boson was CP-violating it would not be an eigenstate.

But especially a CP-violation would be of particular interest since the CP-violation caused by the CKM-matrix is too small to explain the disequilibrium of matter and antimatter in the universe.

The CP-nature of a particle can be investigated through the transversal spin-correlations of its decay particles. This requires that the decay-particles themselves are unstable and decay.

Investigation of Spin and CP The properties spin and CP manifest themselves in different angular distributions and can therefore be investigated by the help of these distributions. In figure 1(a) the distribution of $\cos\theta$ is shown for the SM-hypothesis (red, solid line) and an alternative spin-2-hypothesis (blue, dashed line) with same CP in the channel $H \to \gamma\gamma$. Here θ is the angle between one of the outgoing photons and the z-axis in the Higgs-Boson rest-frame. Since the two photons are back-to-back in the rest frame the angle is the same for both photons. The distribution for the SM-hypothesis is uniform because the Higgs-Boson is a scalar particle in the SM and therefore decays isotropically in its rest-frame.

In figure 1(b) the distributions in the angle ϕ are shown for the SM-hypothesis (black, solid line) and an alternative spin-0-, but CP-odd-hypothesis (red, dashed line) for the channel $H \to ZZ \to 4\ell$. The angle ϕ is the angle between the two Z-Boson decay planes. The planes are spanned by the flight directions of the two leptons in the Z-Boson rest frame.

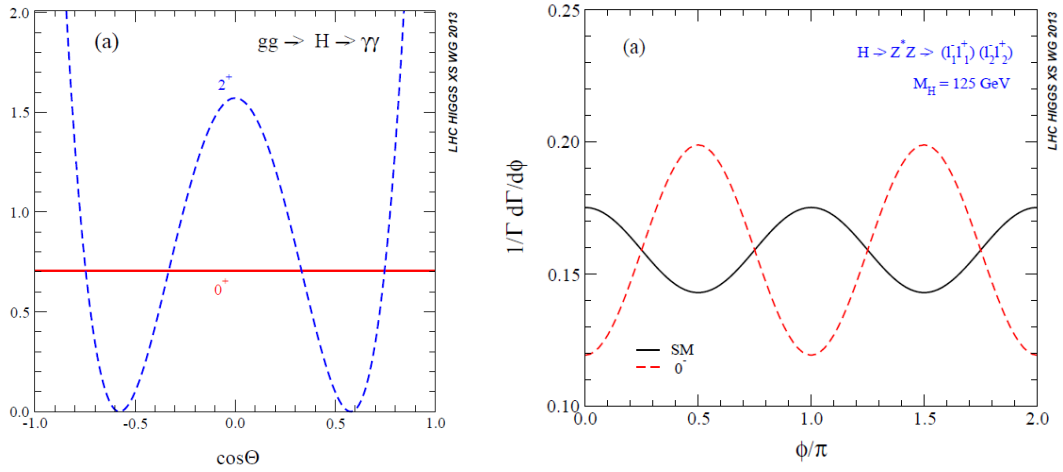

Figure 1: *Example-distributions for the investigation of spin and CP. On the left hand side the distribution in* $\cos\theta$ *is shown for the SM-hypothesis and an alternative spin-2-hypothesis with same CP in the channel* $gg \to H \to \gamma\gamma$*. On the right hand side the distribution in* ϕ *is shown for the SM-hypothesis and an alternative CP-odd-hypothesis with same spin in the channel* $gg \to H \to ZZ \to 4\ell$*. Both figures are from [1]*

In both plots one can clearly see the different curve shapes for the different models.

A short overview of the different alternative hypotheses Besides the SM-hypothesis 0^+ the alternative hypotheses shown in table 1 were tested.

Not every hypothesis was tested in all analyses that are presented later.

The hypotheses do not just differ in spin and CP but also represent different models which one can especially see when looking at the spin-2-models.

To get an idea where these models come from the general scattering amplitude for the interaction of a Higgs-like spin-0 boson with two gauge bosons is shown in equation 1,

0^-	pseudo-scalar
0_h^+	non-SM scalar with higher-dim. operators
1^+	exotic pseudo-vector
1^-	exotic vector
2_m^+	graviton-like tensor with minim. couplings
2_b^+	graviton-like tensor with SM in the bulk
2_h^+	tensor with higher-dim. operators
2_h^-	pseudo-tensor with higher-dim. operators

Table 1: *The alternative hypotheses which are considered in the different analyses.*

from [1].

$$A\left(X_{J=0} \rightarrow VV\right) = \tag{1}$$
$$v^{-1}\left(g_1 m_V^2 \epsilon_1^* \epsilon_2^* + g_2 f_{\mu\nu}^{*(1)} f^{*(2),\mu\nu} + g_3 f^{*(1),\mu\nu} f_{\mu\alpha}^{*(2)} \frac{q_\nu q^\alpha}{\Lambda^2} + g_4 f_{\mu\nu}^{*(1)} \tilde{f}^{*(2),\mu\nu}\right)$$

The $f^{(i),\mu\nu} = \epsilon_i^\mu q_i^\nu - \epsilon_i^\nu q_i^\mu$ are the filed strength tensors of a gauge boson with polarization ϵ_i and momentum q_i. $\tilde{f_{\mu\nu}^{(i)}}$ denotes the conjugate of the field strength tensor. Furthermore there is the vacuum expectation value v and the energy scale of new physics Λ. The coupling term with g_3 is small and can therefore be neglected. The terms with g_1 and g_2 correspond to a scalar (spin=0 and CP-even), g_1 to leading-order (model 0^+) and g_2 to next-to-leading order (model 0_h^+). The term with g_4 corresponds to a pseudo-scalar, i.e. spin=0 and CP-odd and therefore to 0^-. Depending on which coupling terms are considered one can construct different models. Similar scattering amplitudes can be written down for the other spin-hypotheses and models can be constructed.

3 Analysis $H \rightarrow \gamma\gamma$ with ATLAS

The description of this analysis is based on two papers, [2] and [3].

Data corresponding to an integrated luminosity of $20.7\,\text{fb}^{-1}$ at a center-of-mass-energy $\sqrt{s} = 8\,\text{TeV}$ was considered.

The SM-hypothesis 0^+ is compared to a "graviton-like" model with minimal couplings 2_m^+. Since the two photons are stable it is just possible to analyse the longitudinal spin-correlations and therefore just the spin-nature of the boson.

The branching ratio of $H \rightarrow \gamma\gamma$ is quite small. For a Higgs-Boson mass of 125 GeV it is $BR(H \rightarrow \gamma\gamma) = 2.28 \cdot 10^{-3}$, from [1]. Additionally the background of non-resonant diphoton production is large. Nevertheless the significance in this channel is high.

Signal processes The Feynman-diagrams for the signal-processes (0^+ and 2_m^+) are shown in figure 2. On the left hand side one can see the standard-model process with production

mainly via gluon-gluon-fusion and decay to two photons via mainly a top-loop (since the Higgs-Boson couples to mass). On the right hand side one can see the two different considered production modes for the alternative hypothesis. The analysis is performed with different assumptions for the fractions of these two production modes (gluon-gluon-fusion and $q\bar{q}$-annihilation).

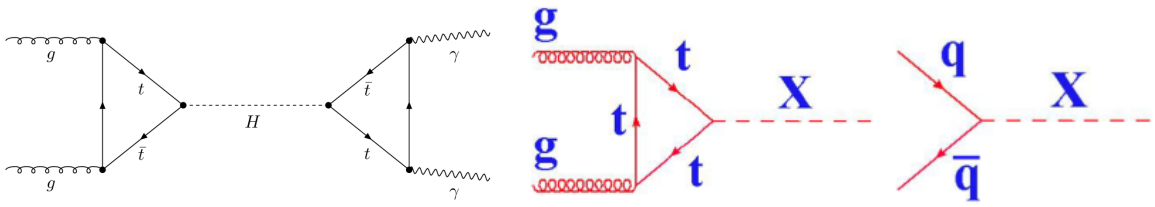

Figure 2: *The two signal-processes, on the left hand side for the SM-hypothesis (from [4]), on the right hand side for the alternative hypothesis (from [5]).*

Background processes The main background-processes, which are irreducible, shown in figure 3, are non-resonant diphoton productions. Furthermore there are several reducible backgrounds like $\gamma + jet$, $jet + jet$, etc.

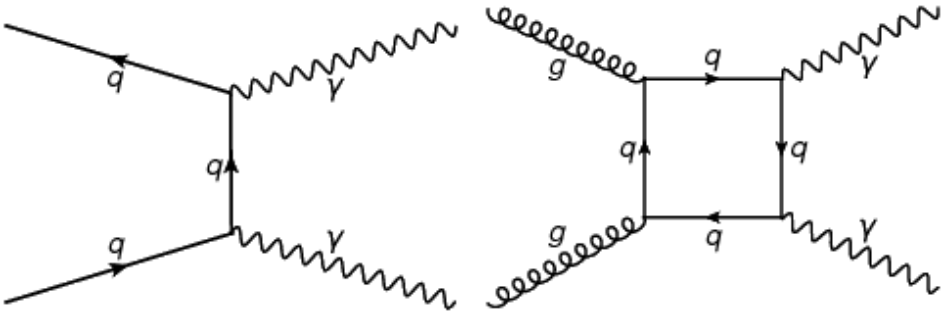

Figure 3: *The two signal-processes, on the left hand side for the SM-hypothesis, on the right hand side for the alternative hypothesis. Both figures are from [6]*

Sensitive observable The sensitive observable in this analysis is the distribution of $|\cos\theta^*|$. The angle θ^* is the polar angle in the Collins-Soper frame, which will be explained in the next paragraph. Since the Collins-Soper frame is defined in the Higgs-Boson rest frame the two photons fly apart back-to-back. That means that there is only one angle to define an hence just one angular observable. The theoretical distributions of this observable for both of the hypotheses was already shown in figure 1(a) and it was also mentioned that the SM-distribution is assumed to be uniform since the SM-Higgs-Boson is scalar and therefore decays isotropically.

The experimental distributions are shown in figure 4. In blue one can see the SM-model. The distribution is not uniform anymore since several cuts were already applied. The alternative model is plotted in red. The solid line is for production only via gluon-gluon-fusion (ggf) and the dashed line for production only via $q\bar{q}$-annihilation. In black the background is shown. The distribution of the 100 % production via ggf is similar to the background and the one of 100 % production via $q\bar{q}$ is SM-like.

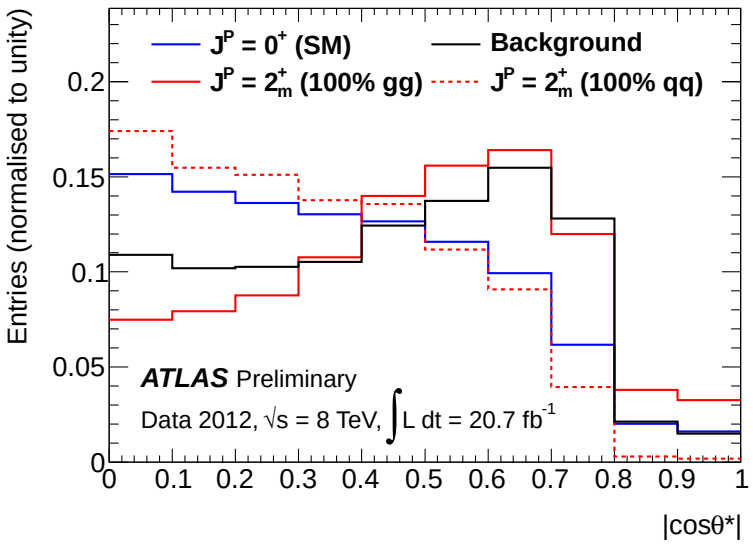

Figure 4: *The distributions in $|\cos\theta^*|$ for the SM-model (blue), the alternative model (red and solid for production only via ggf, red and dashed for production only via $q\bar{q}$) and the background (black) after performing several cuts. Plot from paper [2].*

Collins-Soper frame For the definition of the Collins-Soper frame the choice of the frame of reference and of the z-axis is crucial. In this case the rest-frame of the Higgs-boson (which is equal to the rest-frame of the two photons) is chosen. The z-axis is equal to the bisecting line of the angle between the incoming proton and the negative direction of the other incoming proton, as shown in figure 5. The angle θ^* is between one of the outgoing photons and the new-defined z-axis.

One could think that the two incoming protons also should be in one line but that is just true for the two participating partons but not for the protons.

The advantage of the Collins-Soper frame is that this choice of an angle is less sensitive to initial state radiation of the incoming partons.

In the Collins-Soper frame $|\cos\theta^*|$ depends on the transverse momenta of the two photons $p_T^{\gamma i}$, on the transverse momentum $p_T^{\gamma\gamma}$ and the invariant mass $m_{\gamma\gamma}$ of the two-photon-system and on the difference of the pseudorapidity between the two photons $\Delta\eta^{\gamma\gamma}$ as in equation 2.

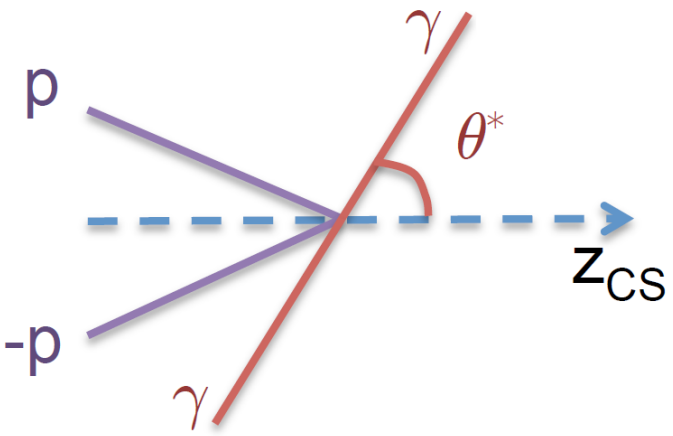

Figure 5: *For the illustration of the Collins-Soper frame.*

$$|\cos\theta^*| = \frac{|\sinh(\Delta\eta^{\gamma\gamma})|}{\sqrt{1+\left(p_T^{\gamma\gamma}/m_{\gamma\gamma}\right)^2}} \frac{2p_T^{\gamma 1}p_T^{\gamma 2}}{m_{\gamma\gamma}^2} \tag{2}$$

Event selection First of all the events of interest have to be selected. For this purpose the following cuts are applied:

- Diphoton trigger with $E_{T,\gamma 1} > 35\,\text{GeV}$ and $E_{T,\gamma 2} > 25\,\text{GeV}$
- $0 < |\eta| < 1.37$ and $1.56 < |\eta| < 2.37$ (Both photon candidates shall be in the fiducial region of the electromagnetic calorimeter but not in the transition region between barrel and endcap.)
- $105\,\text{GeV} < m_{\gamma\gamma} < 160\,\text{GeV}$
- $p_{T,\gamma 1}/m_{\gamma\gamma} > 0.35$ and $p_{T,\gamma 2}/m_{\gamma\gamma} > 0.25$

The relative cuts on $p_{T,\gamma i}/m_{\gamma\gamma}$ shall minimize the correlations between $m_{\gamma\gamma}$ and $\cos\theta^*$ compared to fixed cuts on p_T. The connection between $m_{\gamma\gamma}$ and $\cos\theta^*$ can be seen in equation 2, especially in the second fraction.

Furthermore a mass signal region (SR) and a side band region (SBR) are defined. For the signal region the invariant two photon mass range of $122 - 130\,\text{GeV}$ is chosen, for the side band region the two ranges $105\,\text{GeV} < m_{\gamma\gamma} < 122\,\text{GeV}$ and $130\,\text{GeV} < m_{\gamma\gamma} < 160\,\text{GeV}$. In figure 6 one can see the distribution of the invariant mass of the two photons for motivating the selection of the regions.

Analysis In figure 7 the distribution of the sensitive observable $|\cos\theta^*|$ is shown. The black dots are the measured data, in yellow one can see the estimated background and in cyan the expected signal for the SM-hypothesis. Since the background is assumed to be

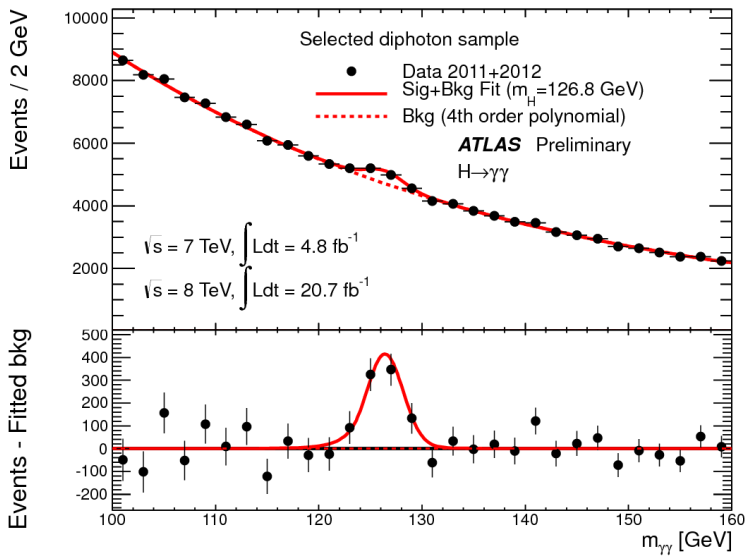

Figure 6: *The distribution of the invariant mass of the two photons. In the upper plot the black dots are the data (signal plus background) and in the lower plot the background is already subtracted. The plot is from paper [7].*

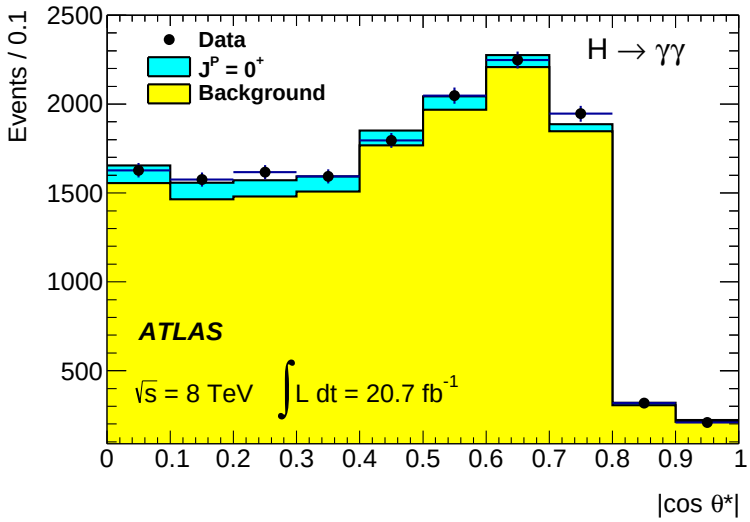

Figure 7: *Distribution of the sensitive observable. In yellow one can see the assumed background an in cyan the SM-signal. The black dots indicate the data. The plot is from paper [3].*

very large compared to the signal a very good estimation of the background is important. That means that the shape of the distribution (f_B) and the yield of the background (n_B) is needed for the invariant mass $m_{\gamma\gamma}$ and the sensitive observable $|\cos\theta^*|$. Furthermore the expected signal for the two hypotheses is estimated as well. The observable $|\cos\theta^*|$ is the sensitive observable and the invariant mass $m_{\gamma\gamma}$ is used to separate signal from

background.

First it is discussed how to obtain the shape of the invariant mass distribution, that means to obtain a probability density function (pdf). Since the natural width of the invariant mass peak is smaller than the experimental resolution it does not make sense to distinguish between the two different signal hypotheses and hence the pdf $f_S(m_{\gamma\gamma})$ is the same for the SM and the spin-2 hypothesis. The pdf $f_S(m_{\gamma\gamma})$ is determined from a fit to a Monte Carlo-simulated distribution. The fit function is the sum of a Crystal Ball and a wider Gaussian function. The pdf for the background $f_B(m_{\gamma\gamma})$ is determined from a fifth-degree polynomial fit to data. The red dashed line in figure 6 corresponds to this fit. However, in the plot it is written that the fit is a fourth-degree polynomial, that is just because the plot is from another paper and another analysis.

The signal shape $f_S(|\cos\theta^*|)$ for $|\cos\theta^*|$ is determined from Monte Carlo simulations for both hypotheses separately . The background shape $f_B(|\cos\theta^*|)$ is determined from the data distribution in $|\cos\theta^*|$ while just considering the events that are in the mass side band region. This is just possible because of de-correlation between $m_{\gamma\gamma}$ and $|\cos\theta^*|$.

For testing the de-correlation, one looks at figur 8. That is not a proof of de-correlation but a visualisation. In the paper they also tested the correlation quantitatively. On the

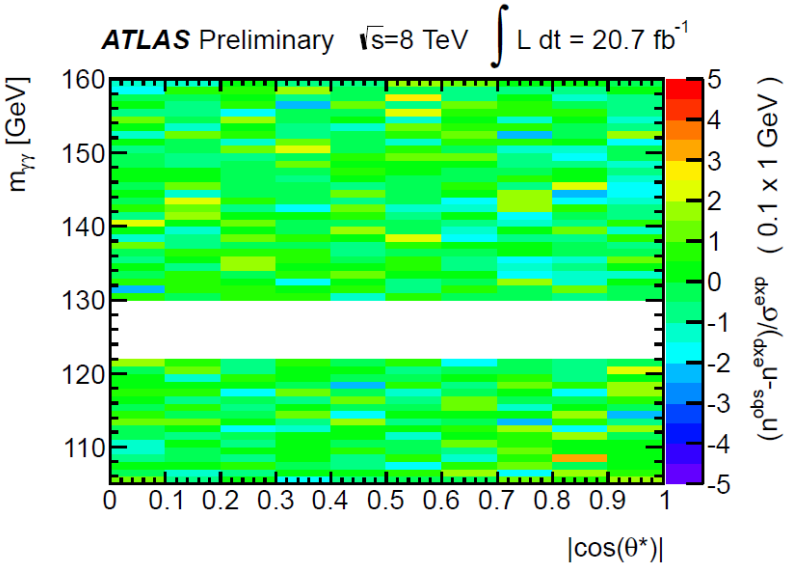

Figure 8: *A plot for visualising the de-correlation between $m_{\gamma\gamma}$ and $|\cos\theta^*|$. It is a two-dimensional binned plot of these two observables while the colours indicate the value of the difference of the number of observed events minus the number of expected events weighted with the uncertainty. Since the colours are more or less randomly distributed one can assume a de-correlation. The mass signal-region is left out. The plot is from paper [2].*

x-axis $|\cos\theta^*|$ is plotted, on the y-axis the invariant mass $m_{\gamma\gamma}$. The colour in each bin indicates the value of the term $(n^{\text{obs}} - n^{\text{exp}})/\sigma^{\text{exp}}$, i.e. the difference of the observed and expected number of events weighted with the uncertainty of the expected events. Green means no difference and blue and red correspond to a greater difference. The

signal region is left out since for the estimation of the background shape $f_B(|\cos\theta^*|)$ just the data in the side band regions are considered (see above). If there was a correlation between the two observables one could see some kind of systematic in the distribution of the colours but they are distributed randomly more or less which means that the observables are de-correlated in good approximation.

Now everything is done to perform a likelihood-fit on the data (for each hypothesis) and hence to obtain the signal and background estimations.

The likelihood function for this analysis under the assumption of de-correlation between $m_{\gamma\gamma}$ and $\cos\theta^*$ is shown in equation 3.

$$\ln\mathcal{L} = -(n_S + n_B) + \sum_{\text{events}} \ln\left[n_S \cdot f_S\left(|\cos\theta^*|\right) \cdot f_S\left(m_{\gamma\gamma}\right) + n_B \cdot f_B\left(|\cos\theta^*|\right) \cdot f_B\left(m_{\gamma\gamma}\right)\right] \tag{3}$$

n_S and n_B are the number of signal respectively background events. They are parameters and estimated from the likelihood-fit. The values of the pdfs $f_S(|\cos\theta^*|)$, $f_S(m_{\gamma\gamma})$, $f_B(|\cos\theta^*|)$ and $f_B(m_{\gamma\gamma})$ are evaluated for each event. The signal pdf $f_S(|\cos\theta^*|)$ is the only input value that changes when evaluating the likelihood function for the different hypotheses.

The first summand is the poisson-factor. It appears since in the maximum-likelihood fit the number of signal and background events is determined simultaneously with the constrain that they should sum up to the total number of events. This constrain is considered in the likelihood-function with a poisson-factor (summand in the log-likelihood) since the probability density function that one really observes n events at an expectation value λ is the poisson-distribution.

Furthermore in practice more terms are added for taking several uncertainties into account.

In figure 9 the now estimated background (by the help of the likelihood-fit) is subtracted from the data in the signal region. The left plot is for the SM-hypothesis, the right one for the alternative model. The dots are background-subtracted data, the solid lines the expected signal distributions and the cyan shaded areas the background uncertainty.

The data points in the left and the right plot differ a little bit. The reason for this is that the number of background events is an estimator of the likelihood-function and therefore depends on the considered hypothesis (on the pdf $f_S(|\cos\theta^*|)$.

One can already see in these plots that the data fit the expected distribution of the SM better than the alternative model. But for a quantitative analysis a hypotheses test is applied. Therefore a test-statistic q is defined in equation 4.

$$q = \ln\mathcal{L}_0(\hat{\theta}_0) - \ln\mathcal{L}_2(\hat{\theta}_2) = \ln\frac{\mathcal{L}_0(\hat{\theta}_0)}{\mathcal{L}_2(\hat{\theta}_2)} \tag{4}$$

The $\hat{\theta}$ are the estimators of the likelihood-function. $\mathcal{L}_0$ is the likelihood-function evaluated under the assumption of the SM-hypotheses and $\mathcal{L}_2$ under the assumption of the spin-2 hypothesis.

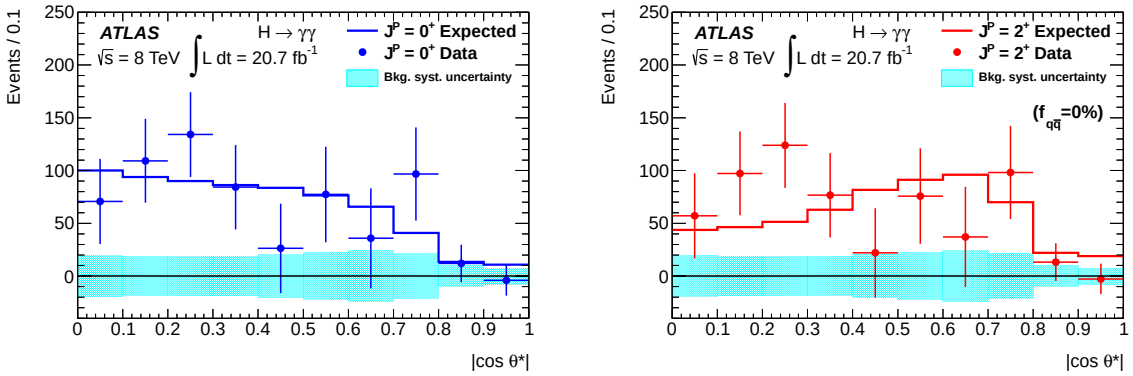

Figure 9: *The dots are the background-subtracted data (signal), the solid lines are the expected signal distributions. The cyan shaded are is the background uncertainty. Just data in the SR is conseidered. On the left hand side is the plot for the SM-hypothesis, on the right hand side for the alternative spin-2 hypothesis (100 % ggf-production). Both plots are from paper [3].*

The plot of the test-statistic q under the two different assumptions is shown in figure 10. In this plot the production mode for the alternative hypothesis is 100 % gluon-gluon-fusion. The red distribution is the one for the SM-hypothesis, the blue one for the alternative one. They are obtained from pseudo-experiments assuming either the SM-hypothesis or the alternative one. The dashed vertical lines are the medians of the distributions and the black solid line is the value of q evaluated from data.

One can see that the data (black line) fit the SM-hypothesis (blue) very well. For a quantitative description a p-value as well as a spin-2 exclusion limit ($1 - CL_S(2^+)$) can be evaluated.

Results The p-value $p(0^+)$ of the SM-hypothesis is calculated by integrating over the blue curve from minus infinity up to the black data line (in figure 10). The p-value $p(2^+)$ of the alternative model is calculated by integrating over the red curve from plus infinity up to the black data line. The test-statistic q was constructed in such a way that the curve of the SM-hypothesis is always at higher values. Furthermore expected p-values can be calculated. For $p_{\text{exp}}(0^+)$ under the assumption that the alternative hypothesis is true one integrates over the blue curve from minus infinity up to the red median (of the alternative hypothesis) and for $p_{\text{exp}}(2^+)$ under the assumption that the SM-hypothesis is true one integrates over the red curve from plus infinity up to the blue (SM) median. For this analysis the p-values shown in equations 5 are obtained.

$$\begin{aligned} p(0^+) = 58.8\,\% \quad &\text{and} \quad p(2^+) = 0.3\,\% \\ p_{\text{exp}}(0^+) = 1.2\,\% \quad &\text{and} \quad p_{\text{exp}}(2^+) = 0.5\,\% \end{aligned} \tag{5}$$

As one can see the p-value and the expected p_{exp}-value for the spin-2 hypothesis fit together well whereas the two values for the spin-0 hypothesis do not fit together. This

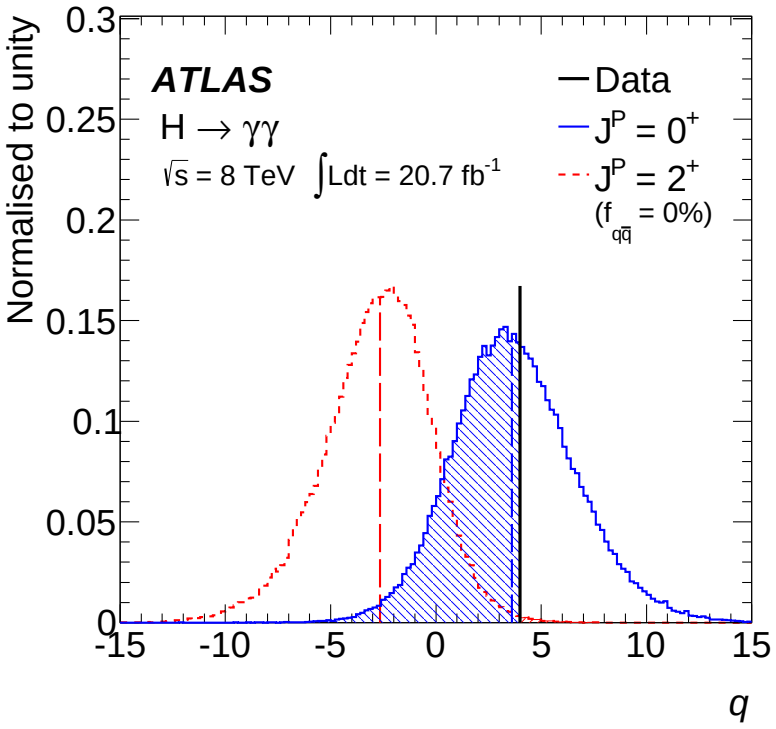

Figure 10: *The distributions of the test-statistic q for the two different hypotheses. In red the SM-hypothesis, in blue the 100 % ggf-produced alternative hypothesis. The dashed vertical lines are the medians of the distributions. The black solid line is the value of q evaluated from the data. The plot is from paper [3].*

favours the spin-0 model. Additionally the $p(0^+)$-value is close to 50 % (respectively even greater) which corresponds to the median.

The spin-2 exclusion limit $1 - CL_S(2^+)$ is defined and has a value as shown in equation 6.

$$1 - \mathrm{CL_S}(2^+) = 1 - \frac{p(2^+)}{1 - p(0^+)} = 99.3\,\% \tag{6}$$

That means that the spin-2 hypothesis can be excluded at a confidence level of 99.3 %. This exclusion limit was defined ad-hoc to avoid that one hypothesis is rejected/favoured because of the p-value while the two test-statistic curves are so similar that they are nearly equal (very low significance). If they were completely equal the $p(0^+)$-value plus the $p(2^+)$-value would be equal to one. That would mean that $1 - p(0^+)$ is equal to $p(2^+)$ and therefore the spin-2 exclusion limit would be zero (although $p(0^+)$ could still be 58.8 %).

Comparison of different fractions of the two spin-2 production modes As written in the beginning two different production modes are considered for the alternative

hypothesis. These are gluon-gluon-fusion and $q\bar{q}$-annihilation. It was analysed how the different fractions influence the significance of the analysis and thus the exclusion limits. In figure 11(a) one can see the medians of the test-statistic q-distributions (y-axis) for different fractions of $q\bar{q}$-annihilation (y-axis). The dots in black are the evaluated

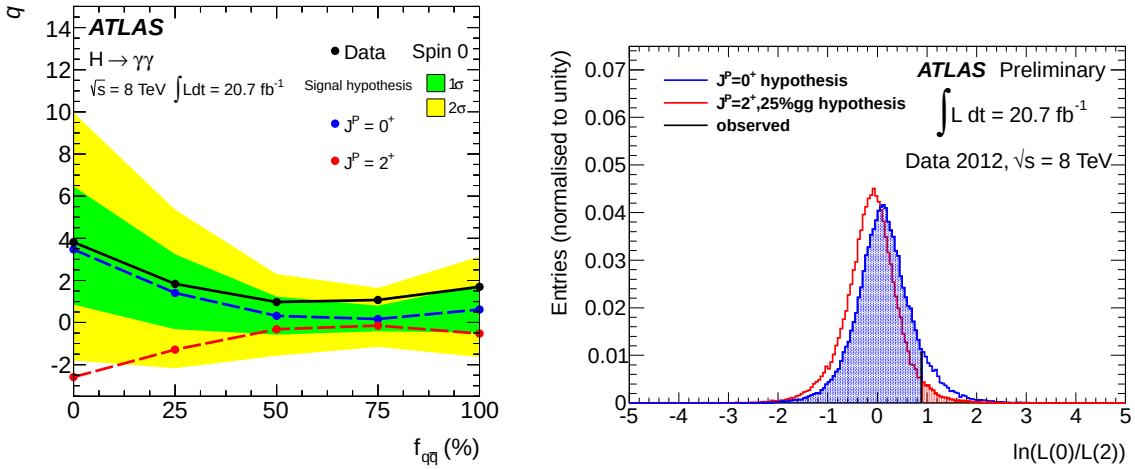

Figure 11: *In the left picture different values for the production fraction of $q\bar{q}$-annihilation is plotted on the x-axis while on the y-axis q is plotted. The blue and red dots correspond to the means of the q-distributions of the SM (blue) and the alternative hypothesis (red). The black dots are the values in data. The green and yellow areas indicate the 1σ and 2σ areas around the SM-values. The difference of the red and blue dots is a measure for the sensitivity. The plot is from paper [3]. In the right plot one can see the different q-distributions (SM: blue and alternative: red) for a production fraction of 75 % of $q\bar{q}$-annihilation. This plot is from paper [2].*

values for q from the data. The red dots are the values of the median of the respective q-distribution of the alternative hypothesis, in blue the same for the SM. The green area is the 1σ-, the yellow is the 2σ-area around the SM-values. One can see that the 'q-distance' of the blue and red dots is at its maximum where $f_{q\bar{q}} = 0\,\%$ and at its minimum where $f_{q\bar{q}} = 75\,\%$. In figure 11(b) one can see the distributions of the test-statistic q for $f_{q\bar{q}} = 75\,\%$. The two distributions are nearly equal and therefore the significance is very low. The observed q-value from the data is not very good to see (ca. $q \approx 0.9$). The p-value of the SM-hypothesis is $p(0^+) = 90.2\,\%$, but the exclusion limit is only $1 - \mathrm{CL_S} = 66.3\,\%$. And hence the alternative hypothesis cannot be rejected.

Results from CMS In this paragraph the results from CMS in the analysis $H \to \gamma\gamma$ are shortly introduced. They used an integrated luminosity of $19.6\,\mathrm{fb}^{-1}$ at a center-of-mass energy of $\sqrt{s} = 8\,\mathrm{TeV}$. The corresponding paper is [8]. They also used $|\cos\theta^*|$ as sensitive observable. In figure 12(a) and 12(b) the distributions of the test-statistic are shown, left for 100 % gluon-gluon-fusion and right for 100 % $q\bar{q}$-annihilation. The test-statistic is defined slightly different (factor of 2). The yellow distributions correspond to the SM-hypothesis, the blue distributions to the alternative one. The red arrows indicate the observed values

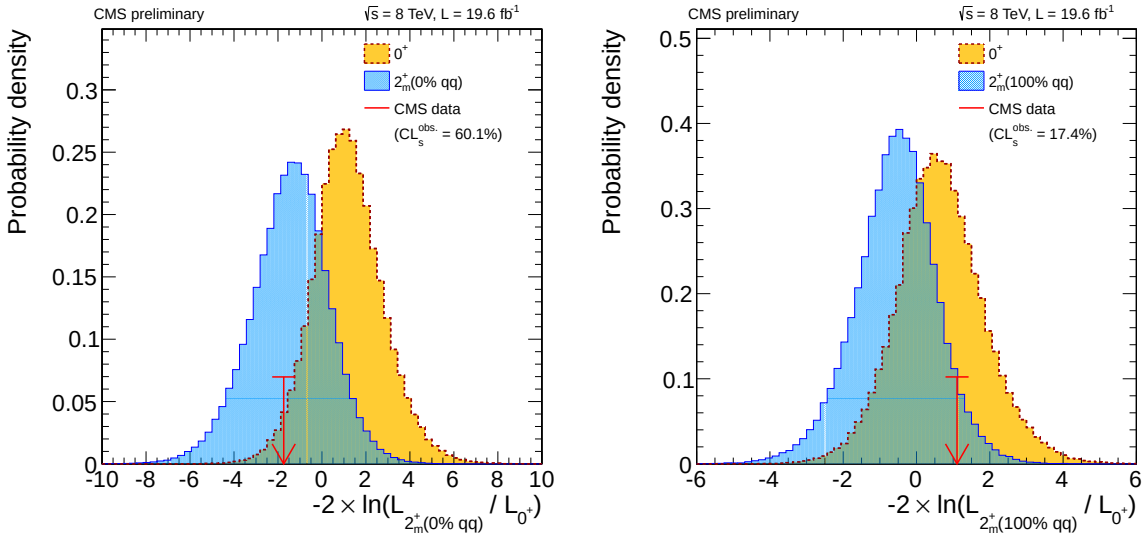

Figure 12: *In both plots one can see the distributions of the test-statistic q. In yellow for the SM-hypothesis and in blue for the alternative one. The red arrows indicate the values in data. The left plot is for a fraction of 0 % $q\bar{q}$-annihilation production the right one for a fraction of 100 %. Both plots are from paper [8].*

in data.

The spin-2 exclusion limits are shown in equation 7.

$$\begin{aligned} 100\,\%\ ggf: &\quad 1-\mathrm{CL_S}(2^+_m) = 39.1\,\% \\ 100\,\%\ q\bar{q}: &\quad 1-\mathrm{CL_S}(2^+_m) = 83.1\,\% \end{aligned} \tag{7}$$

In both cases the spin-2 hypothesis cannot be excluded.

4 Analysis $H \to ZZ^* \to 4\ell$ with CMS

The description of this analysis is based on the paper [9]. An integrated luminosity of 5.1 fb^{-1} at a center-of-mass energy $\sqrt{s} = 7\,\mathrm{TeV}$ and an integrated luminosity of 19.7 fb^{-1} at a center-of-mass energy $\sqrt{s} = 8\,\mathrm{TeV}$ was considered.

The branching fraction of this channel is very low, of the order of 10^{-4} (see [9]) but all decay products are visible.

The SM-hypothesis 0^+ is compared to eight alternative hypotheses. Since the two Z-Bosons are not stable but decay to the four leptons not just a spin-analysis but also a CP-analysis is possible.

Signal process In figure 13 the feynman-diagram of the signal process with production via gluon-gluon-fusion is shown.

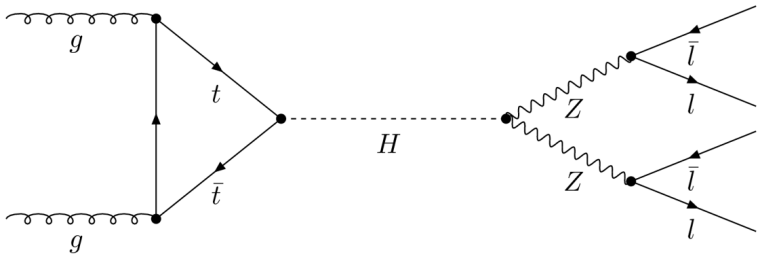

Figure 13: *The feynman-diagram for the SM signal process via gluon gluon fusion, from [4].*

Background processes The main, irreducible background is direct ZZ-production via $q\bar{q}$-annihilation or gluon-gluon-fusion as shown in figure 14(a) and 14(b). These processes are estimated from Monte-Carlo simulations. Subleading, reducible background processes

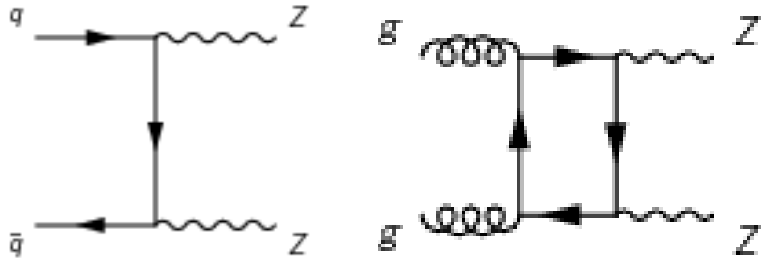

Figure 14: *The direct ZZ-production via ggf or $q\bar{q}$-annihilation is the main irreducible background. The plots are from [10].*

are $Z + jets$, $t\bar{t}$, and $WZ + jets$ estimated from signal-free control regions in data.

Event selection In the beginning the events of interest have to be selected. Two pairs of leptons are required. In this case leptons ℓ are electrons or muons. The leptons in a pair must be opposite charged and of same flavour. Further requirements are:

- $p_T^e > 7\,\text{GeV}$ and $|\eta|^e < 2.5$
- $p_T^\mu > 5\,\text{GeV}$ and $|\eta|^\mu < 2.4$
- $40 < m_{Z1} < 120\,\text{GeV}$
- $12 < m_{Z2} < 120\,\text{GeV}$

Since the mass of both of the Z-Bosons together is greater than the mass of the Higgs-Boson at least one of the Z-Bosons is virtual. The lepton-pair with an invariant mass

closer to the one of a Z-Boson is called the first Z-Boson with the invariant mass m_{Z1} and the other is the second with m_{Z2}.

In figure 15 one can see the invariant mass distribution of the four leptons. The black

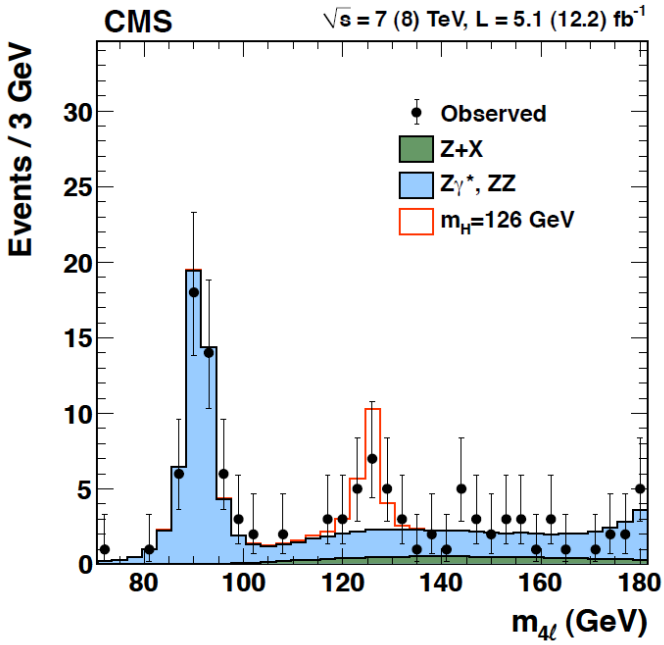

Figure 15: *Here one can see the distribution of the invariant mass of the four leptons. The black dots are the data points. The blue and green shaded areas are the estimated background and in red one can see the estimated signal at a four lepton mass of the Higgs-Boson mass. The plot is from [11].*

dots are the observed data, in blue and green one can see the expected backgrounds. And in red the expected signal at the Higgs-Boson mass is shown. Therefore only events in the mass range $106 < m_{4\ell} < 141\,\text{GeV}$ are considered in the following analysis. The peak in the blue background is at the Z-Boson mass and comes from a Z-Boson that decays into two leptons. One of these leptons is off-shell and radiates away another Z-Boson which also decays into two leptons. All together there are four leptons coming from one Z-Boson making this blue peak.

Sensitive observables To distinguish between the different hypotheses five angles in the four lepton rest-frame are used. They are shown in figure 16. In the Higgs-Boson rest-frame the two Z-Bosons fly apart back-to-back. The angle θ^* is the angle between the direction of the incoming partons and the direction of the corresponding Z-Boson. Then in the rest-frame of the two Z-bosons respectively there are the angles θ_i between one of the back-to-back outgoing leptons and the flight-direction of the Z-Boson with respect to the Higgs-boson rest-frame. The flight-direction of the two leptons in the Z-Boson rest-frame and the flight-direction of the Z-Boson in the Higgs-Boson rest-frame span a plane. Φ_1 is the angle between this plane of the first Z-Boson and the axis of the incoming

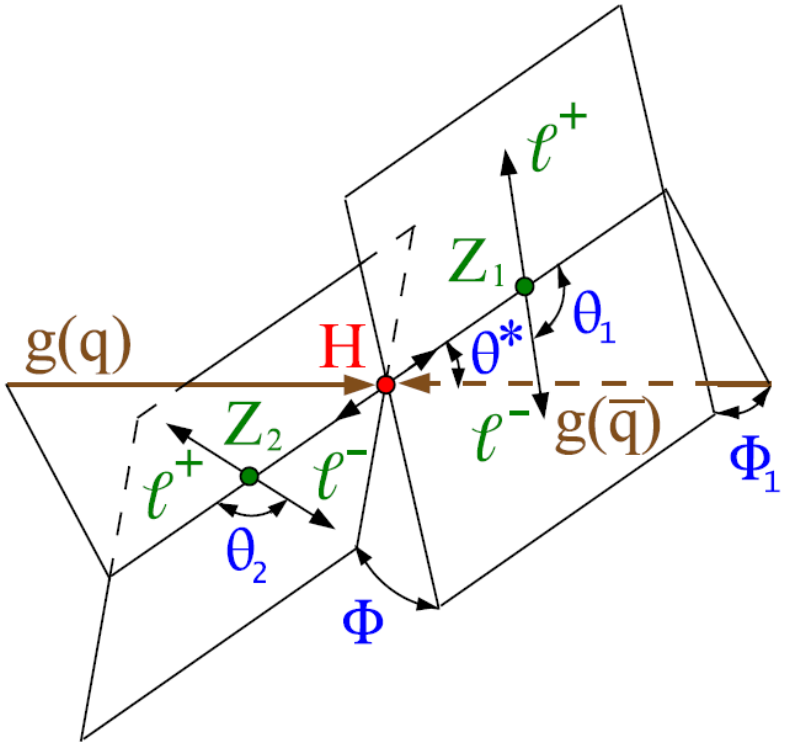

Figure 16: *A sketch to visualise the five angles that are used as sensitive observables in this analysis, from [9].*

parton. The angle Φ is the angle between the plane of the first and the plane of the second Z-Boson.

These five angles together with the masses of the two Z-Bosons, m_{Z1} and m_{Z2} fully describe the kinematic configuration of the 4ℓ-system in its rest frame.

The distribution of four of these five angles are shown in figure 17. But they are from the corresponding analysis of ATLAS. In red and magenta one can see the backgrounds. The two lines correspond to two different hypotheses. In the figures 17(a) and 17(d) the SM-hypothesis and the 0^--hypothesis are compared. In the figures 17(b) and 17(c) two different spin-2 models are compared (2^+_m and 2^-).

One can see that the single variables do not have a great separation power but in combination this can be enhanced. For this purpose a discriminant for separation between signal and background $\mathcal{D}_{\text{bkg}}$ and another for separation between two signal hypotheses $\mathcal{D}_{J^P}$ shall be constructed which base on matrix-elements. For this probability density functions $\mathcal{P}^{\text{kin}}\left(m_{Z1}, m_{Z2}, \vec{\Omega} | m_{4\ell}\right)$ are used which are computed from leading-

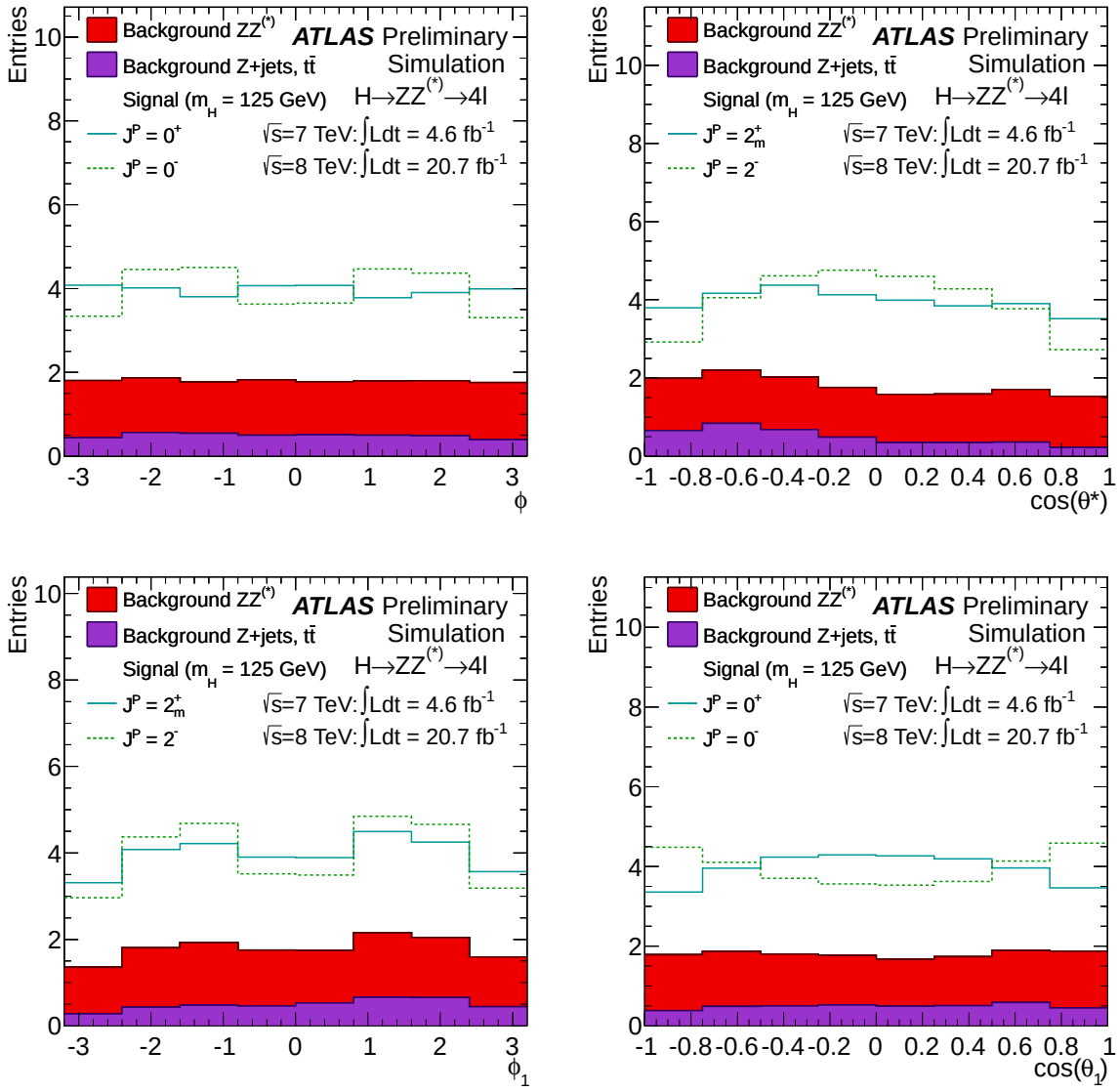

Figure 17: *The distributions of four of the five angles is shown. They are from the corresponding analysis of ATLAS, [12]. In red and magenta one can see the backgrounds and the solid and dashed line are the signal distributions for different hypotheses.*

order matrix-elements squared. Thereby the following $\mathcal{D}$ are obtained:

$$\mathcal{D}_{\text{bkg}} = \left[1 + \frac{\mathcal{P}^{\text{kin}}_{\text{bkg}}\left(m_{Z1}, m_{Z2}, \vec{\Omega}|m_{4\ell}\right) \cdot \mathcal{P}^{\text{mass}}_{\text{bkg}}\left(m_{4\ell}\right)}{\mathcal{P}^{\text{kin}}_{0^+}\left(m_{Z1}, m_{Z2}, \vec{\Omega}|m_{4\ell}\right) \cdot \mathcal{P}^{\text{mass}}_{0^+}\left(m_{4\ell}|m_{0^+}\right)}\right]^{-1} \tag{8}$$

$$\mathcal{D}_{J^P} = \left[1 + \frac{\mathcal{P}^{\text{kin}}_{J^P}\left(m_{Z1}, m_{Z2}, \vec{\Omega}|m_{4\ell}\right)}{\mathcal{P}^{\text{kin}}_{0^+}\left(m_{Z1}, m_{Z2}, \vec{\Omega}|m_{4\ell}\right)}\right]^{-1} \tag{9}$$

The kinetic probability density functions $\mathcal{P}^{\text{kin}}\left(m_{Z1}, m_{Z2}, \vec{\Omega}|m_{4\ell}\right)$ consider the two Z-Boson masses and the five angles for a fixed (given) value of the four-lepton mass ($m_{4\ell}$). The subscripts "bkg", "0^+" and "J^P" indicate the probability functions under the assumption that it is background, the SM-signal or signal of an alternative hypothesis. $\mathcal{P}^{\text{mass}}\left(m_{4\ell}\right)$ is the probability density function (pdf) for the four-lepton mass and $\mathcal{P}^{\text{mass}}\left(m_{4\ell}|m_{0^+}\right)$ the pdf for the four-lepton mass under the assumption that the for-lepton mass is the SM Higgs-Boson mass.

Now all sensitive observables are combined in one. In figure 18 one can see two examples plots of these discriminants. The blue and green shaded areas are background.

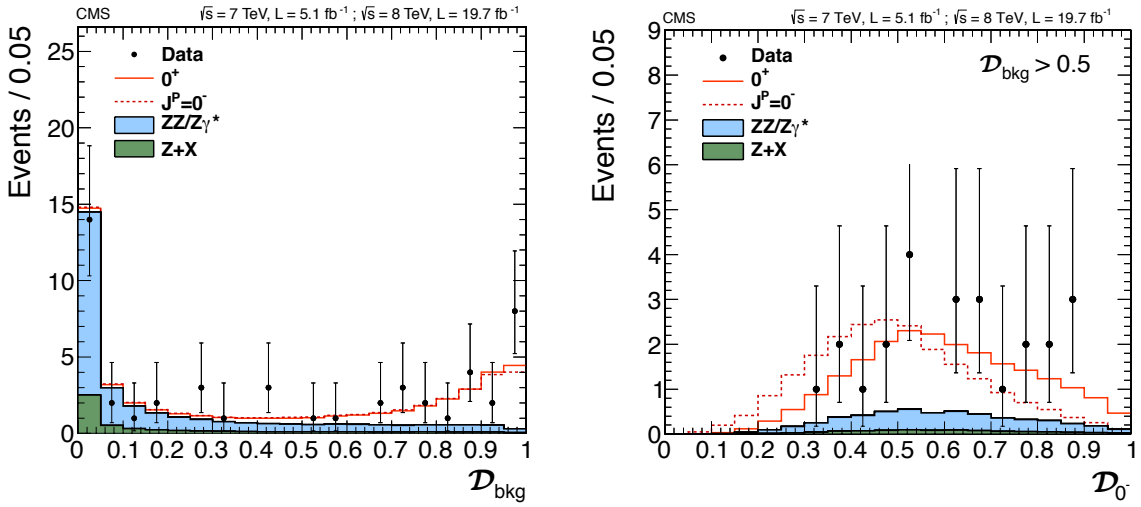

Figure 18: *In this figure the distributions of two of the constructed discriminants are shown. The blue and green shaded areas are background. The black dots are the data points and the red lines are signal, the solid line is for the SM and the dashed line for the alternative model. On the left side one can see the discriminant for separating between signal and background and on the right side the discriminant for separating between SM-hypothesis and 0^--hypothesis. The plots are from [9].*

The black dots are data and the red lines represent the estimated signal distributions. The solid line is the SM-hypothesis and the dashed line for the 0^--hypothesis. In figure 18(a) the distribution of the discriminant separating between signal and background is shown. One can see that the signal distributions are nearly independent of the hypothesis but that there is separation power between signal and background. In figure 18(b) the discriminant for separation between the two hypotheses is shown but only for $\mathcal{D}_{\text{bkg}} > 0.5$ (more signal and less background). This constraint is just applied for plotting but not in the analysis.

Likelihood-function and results For a quantitative conclusion of the analysis a two-dimensional likelihood-function is constructed with these two discriminants for each

hypothesis:

$$\mathcal{L}_{2D}^{J^P} = \mathcal{L}_{2D}^{J^P}(\mathcal{D}_{\text{bkg}}, \mathcal{D}_{J^P}) \tag{10}$$

And is then fitted to data. Furthermore a test-statistic q is defined in equation 11.

$$q = -2\ln(\mathcal{L}_{J^P}/\mathcal{L}_{0^+}) \tag{11}$$

An example plot of the expected distributions in q for two different hypotheses (0^+ and 0^-) obtained from pseudo-experiments is shown in figure 19. In blue one can see the

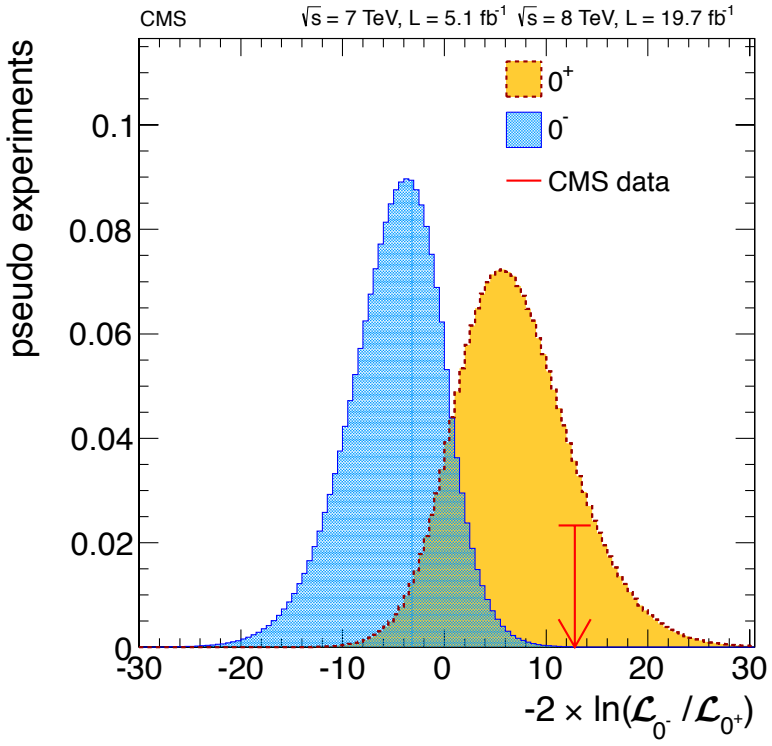

Figure 19: *In this plot one can see the distributions of the test-statistic q. In blue for one alternative model (0^-) and in yellow for the SM. The red arrow indicates the value evaluated from the data. The plot is from [9].*

distribution for the alternative hypothesis 0^- and in yellow for the SM-hypothesis 0^+. The red arrow indicates the value of the data. One can see that the data favour the SM-hypothesis.

Since a lot of models were tested one can see in figure 20 a summary plot for all hypotheses. On the x-axis one can see all the different models and on the y-axis the values for the test-statistic q. For each model we have a black dot which indicates the value for q of the data. The dashed black lines represent the medians of the q-distribution for the different hypotheses. The SM-hypothesis is in orange, the alternative ones in blue. The

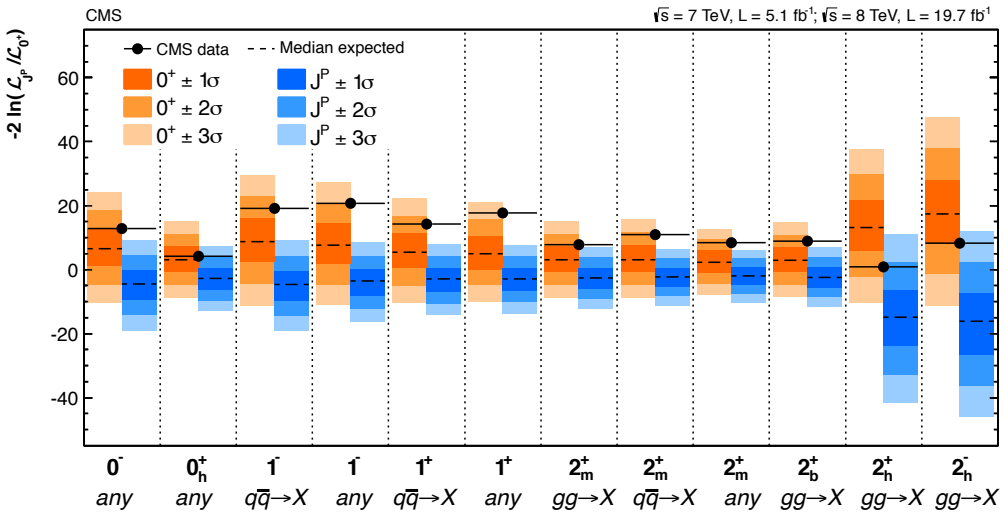

Figure 20: *This plot is also from [9] and shows the the medians (dashed lines) of the q-distributions for all the tested-models (blue) compared to the SM (orange). The shaded areas around the dashed lines correspond to the first three sigma-areas. The dots are the values of q evaluated from data.*

darkest shaded areas are the 1σ-ranges of the q-distribution, the little lighter areas are the ones for the 2σ-range and the lightest for the 3σ-range.

For all but the two last models the data are even more SM-like than expected. For the last two models the data points are still closer to the median of the SM-hypothesis. In the following values for the confidence levels of summarised models are declared:

$$1-\mathrm{CL_S}(0^-,0_h^+) \geq 95.5\,\% \qquad 1-\mathrm{CL_S}(1) \geq 99.98\,\% \qquad 1-\mathrm{CL_S}(2) \geq 97.7\,\% \tag{12}$$

Models with the same assumption for the spin are summarised.

All alternative models can be excluded with a confidence level of at least 95.5 % and therefore rejected.

Results from ATLAS In this paragraph the results from ATLAS in the analysis $H \to ZZ \to 4\ell$ are shortly shown. The corresponding paper is [12] and [3]. An integrated luminosity of $4.6\,\mathrm{fb}^{-1}$ at a center-of-mass energy of $\sqrt{s} = 7\,\mathrm{TeV}$ and $20.7\,\mathrm{fb}^{-1}$ at a center-of-mass energy of $\sqrt{s} = 8\,\mathrm{TeV}$ was used. In this analysis are just four alternative models considered ($J^P = 0^-, 1^+, 1^-, 2^+$). The used sensitive observables are the same as in the CMS-analysis (five angles and the two Z-Boson masses) but the mass-window of the event-selection is a bit smaller ($115 < m_{4\ell} < 130\,\mathrm{GeV}$) and it was not used a matrix-likelihood approach for the combination of the sensitive observables but a boosted decision tree (BDT). With the output of the BDT a likelihood-function was constructed and a test-statistic q defined. An example plot of the q-distributions for the SM-hypothesis versus the alternative model 0^- is shown in figure 21. In red the distribution of the alternative

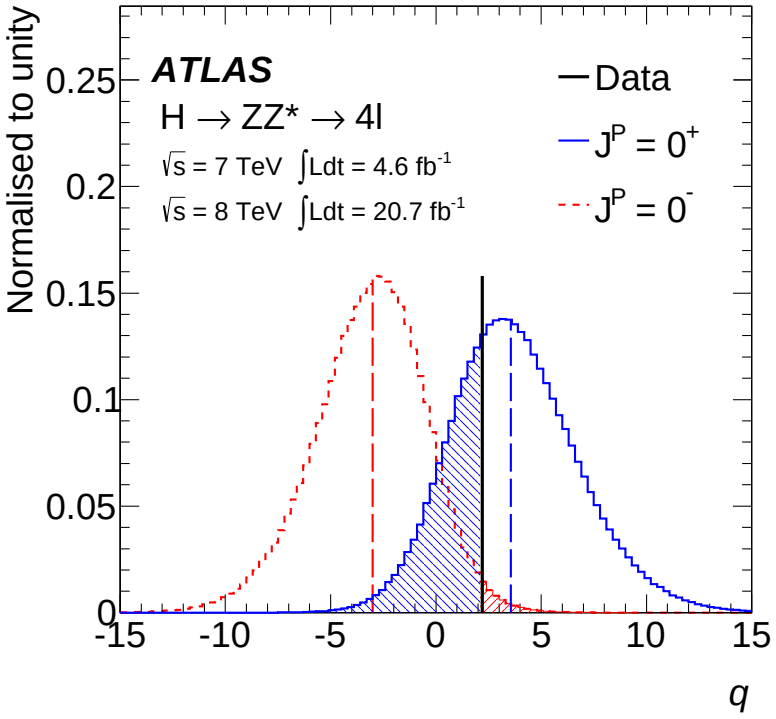

Figure 21: *In this plot one can see the distributions of the test-statistic q for ATLAS. In blue the SM and in red one alternative hypothesis (0^-). The black line indicates the value in data, from [12].*

model is plotted in blue the one of the SM. The dashed lines represent the medians and the black line the value of the data.

The confidence-levels for all tested models are listed in the following:

$$1 - \mathrm{CL_S}(0^-) = 97.8\,\% \qquad 1 - \mathrm{CL_S}(2^+) = 96.4\,\% \tag{13}$$

$$1 - \mathrm{CL_S}(1^+) = 99.8\,\% \qquad 1 - \mathrm{CL_S}(1^-) = 94.0\,\% \tag{14}$$

All models can be excluded at least at a confidence-level of 94 %. For a rejection the critical value for the confidence-level is 95 %.

5 Analysis $H \to WW \to e\nu_e\mu\nu_\mu$ with ATLAS

The basis for the following short description is paper [13] and [3]. An integrated luminosity of 20.7 fb^{-1} at a center-of-mass energy of $\sqrt{s} = 8\,\mathrm{TeV}$ was used. The SM-hypothesis is compared to three alternative hypotheses, 1^+, 1^- and 2^+_m. The analysis is very similar to the ZZ-analysis but in this channel there is missing transverse energy E_T^{miss} in the final state. And hence not all the five angles of the former analysis can be reconstructed. In the final state one electron and one muon is required and not two leptons of the same

flavour since with two different flavours a better separation from background is possible (a Z-Boson would decay into two leptons of the same flavour).

Sensitive observables Because of the missing transverse energy in the final state other sensitive observables are used. That are the the difference of the angles ϕ of the two leptons $\Delta\phi_{\ell\ell}$, the invariant mass of the two leptons $m_{\ell\ell}$, the transverse momentum of the two-lepton-system $p_T^{\ell\ell}$ and the transverse mass of the two leptons and the missing transverse energy m_T which corresponds to the transverse mass of the Higgs-Boson.

The expected distributions of the first three observables are shown in figure 22. In red

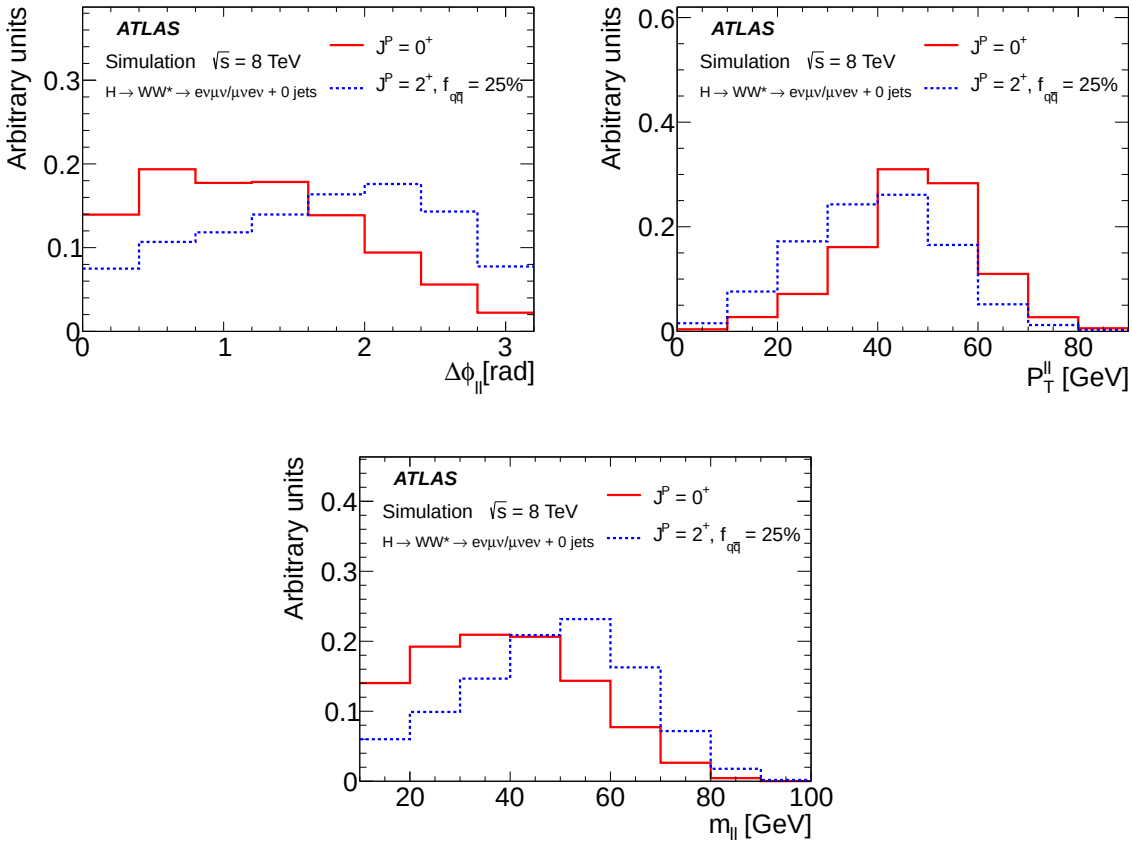

Figure 22: *Three sensitive observables are shown in this figure. The red line corresponds to the SM and the blue dashed line to the 2^+-model with a production mode fraction of 25 % $q\bar{q}$-annihilation. The plots are from [13].*

the distribution for the SM-hypothesis is plotted and in blue the one for the 2^+-alternative hypothesis with a production fraction of $q\bar{q}$-annihilation of 25 %. Furthermore zero jets are required in the event selection to suppress the VBF-production for the SM-signal production.

The distribution of the transverse mass m_T is shown in figure 23 with all the backgrounds, the signal (SM in red) and the data points (black dots). The observable m_T

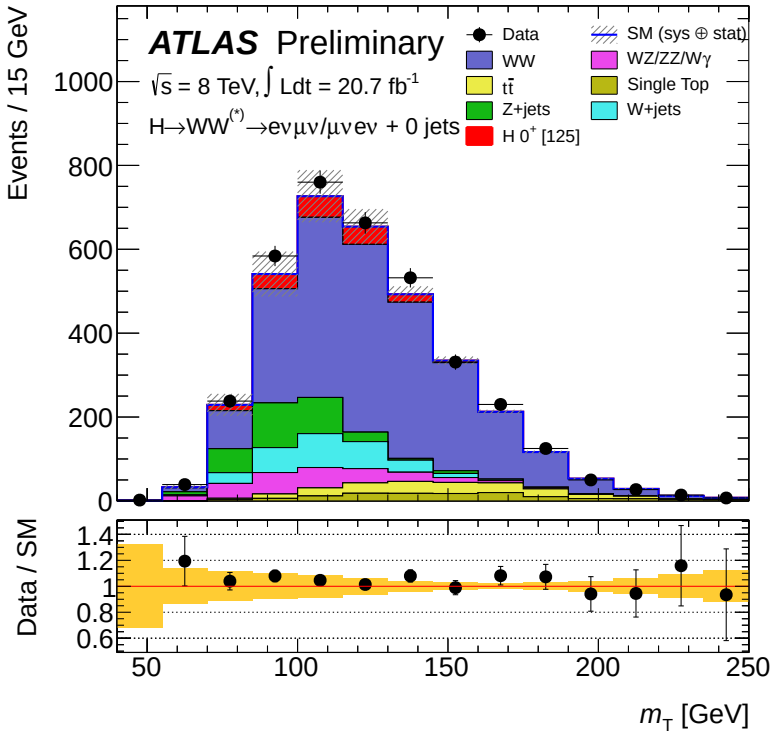

Figure 23: *The distribution of the transverse mass m_T is shown here with backgrounds and data points (black dots) and the expected SM-signal in red, from [13].*

provides mainly separation from background.

Results The four observables are combined in a BDT again, then a likelihood-function is defined and a test-statistic q constructed. The distribution of this test-statistic for the SM-hypothesis compared with all three alternative hypothesis is shown in figure 24. The red distribution is the one of the alternative hypothesis and the blue one of the SM-hypothesis. The black line indicates the q-value of the data. For the 2^+-hypothesis (figure 24(a)) a fraction of 25 % of $q\bar{q}$-annihilation is assumed, furthermore zero jets are required for all hypotheses again. In figure 24(b) the SM-hypothesis is compared to the 1^--model and in figure 24(c) to the 1^+-model.

The corresponding confidence-levels are listed in the following:

$$1 - \mathrm{CL_S}(2^+) = 98.0\,\% \qquad 1 - \mathrm{CL_S}(1^-) = 98.3\,\% \qquad 1 - \mathrm{CL_S}(1^+) = 92\,\% \tag{15}$$

Hence the hypotheses 2^+ and 1^- can be rejected. For the hypothesis 1^+ the confidence-level is smaller than 95 %. One had the same "problem" already in the $H \to ZZ$-analysis with ATLAS (for 1^- instead of 1^+). Therefore it would make sense to combine all the different channels. This is done in the following section at least for ATLAS.

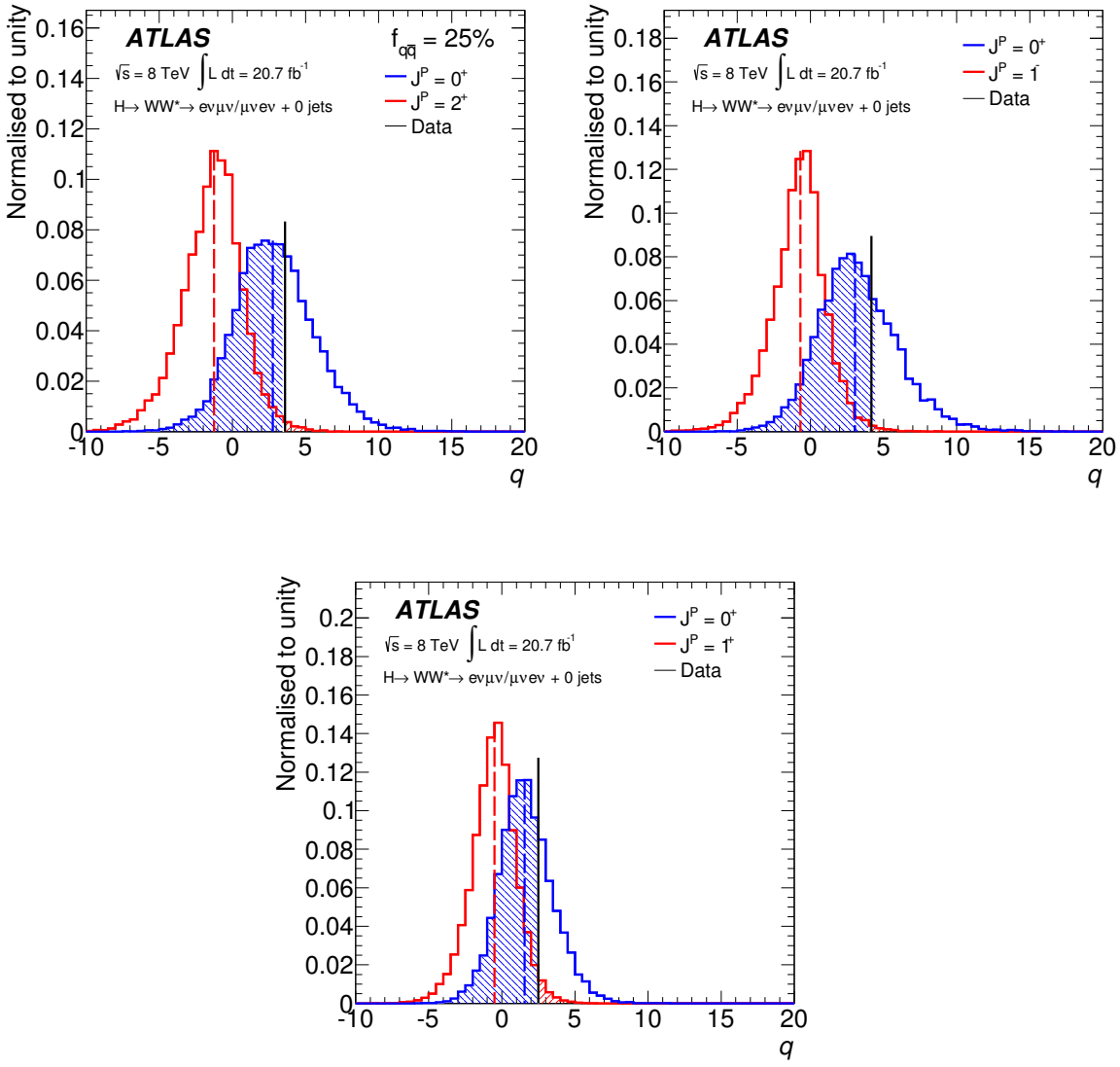

Figure 24: *In this figures the distributions of the test-statistic q are shown for the comparison of the SM (blue) with three alternative hypotheses (red). The black lines indicate the values in data. the plots are from [13]*

6 Combination of the three channels for ATLAS

Combination for the confidence-levels In the following the three channels $H \to \gamma\gamma$, $H \to ZZ \to 4\ell$ and $H \to WW \to e\nu_e\mu\nu_\mu$ are combined. Since not all hypotheses were considered in all three channels one can see a summary in table 2. For the alternative hypothesis 0^- there is just one channel ($H \to ZZ$). For the two spin-1-hypotheses two

	$\gamma\gamma$	ZZ^*	WW^*
0^-		x	
$1^+/1^-$		x	x
2^+	x	x	x

Table 2

channels can be combined and for the 2^+-model all three channels are combined. The resulting confidence-levels are shown in the following:

$$1 - \mathrm{CL_S}(0^-) = 97.8\,\% \qquad 1 - \mathrm{CL_S}(2^+) \geq 99.95\,\% \tag{16}$$

$$1 - \mathrm{CL_S}(1^+) = 99.97\,\% \qquad 1 - \mathrm{CL_S}(1^-) = 99.73\,\% \tag{17}$$

After the combination all tested alternative hypotheses can be rejected.

Investigation of sensitivity dependent on different production modes for the 2^+-model
Another interesting thing to investigate is the influence of the combination of the three channels on the sensitivity to distinguish between the SM-hypothesis and the 2^+-hypothesis for different production modes for the 2^+-model. In figure 25 plots for the sensitivity depending on different fractions of the production modes gluon-gluon-fusion and $q\bar{q}$-annihilation are shown. Such a plot was already shown in figure 11(a) for the channel $H \to \gamma\gamma$ and here in figure 25(a). On the x-axis of the plots different fractions $f_{q\bar{q}}$ are plotted and on the y-axis the q-values. The dots of the dashed lines represent the medians of the q-distributions for the SM-hypothesis (blue) and for the 2^+-hypothesis (red). In black one can see the values evaluated from the data. The green and yellow shaded areas are the 1σ- and 2σ-areas around the mean q-values of the SM-hypothesis. Figure 25(b) is for the $H \to ZZ$-channel and figure 25(c) for the $H \to WW$-channel.

One can see that for the $H \to \gamma\gamma$-channel the sensitivity (difference between blue and red line) is best for $f_{q\bar{q}} = 0\,\%$, for the $H \to ZZ$-channel it is nearly equal for all fractions and for the $H \to WW$-channel the sensitivity is best for a fraction of $f_{q\bar{q}} = 100\,\%$. Thus when combining all three channels the differences in the sensitivities cancel each other nearly out which can be seen in figure 25(d). But the sensitivity is still better for the extreme values of the production mode fractions.

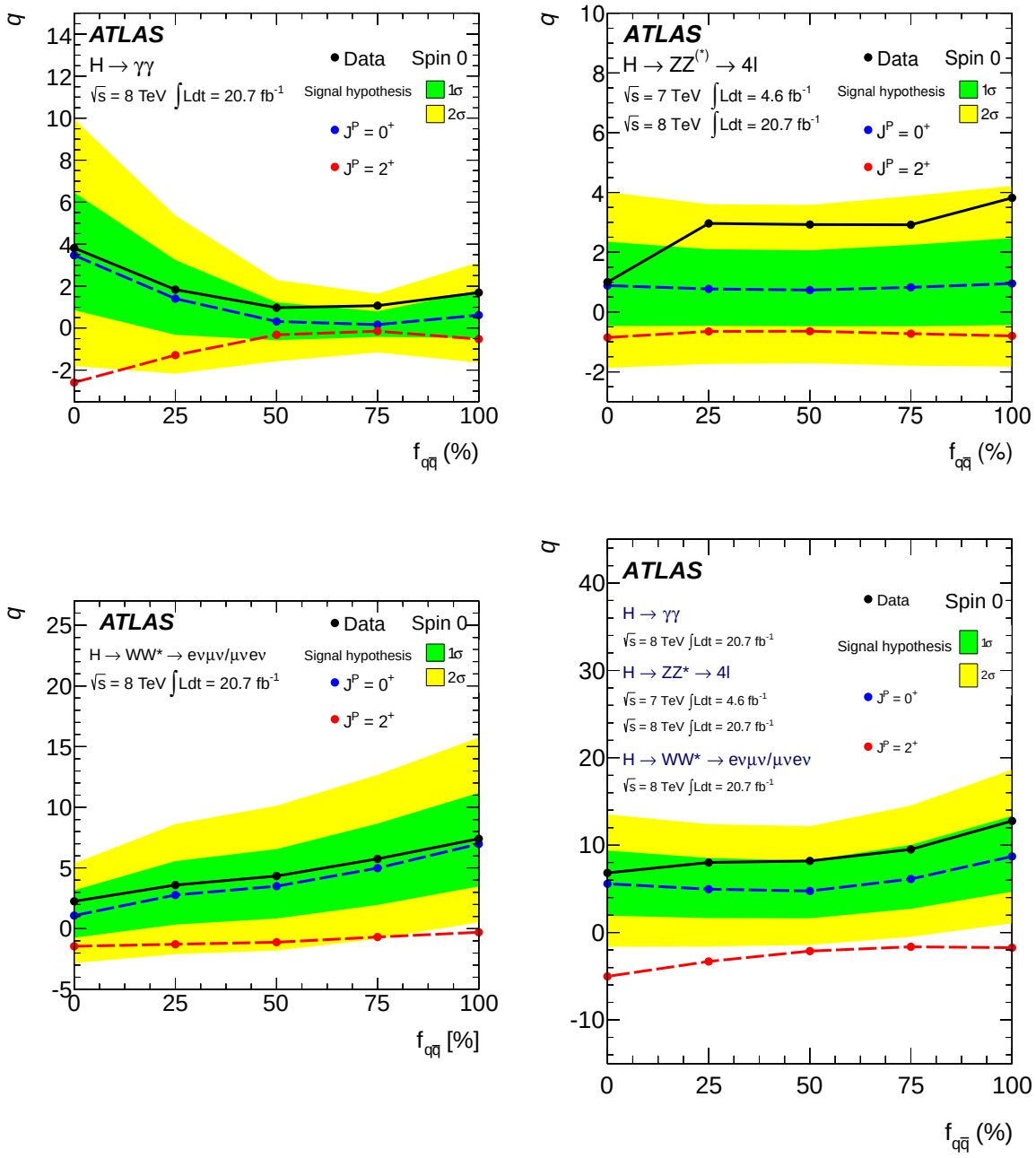

Figure 25: *These figures are from [3]. They show the medians of the q-distributions (dots) for different fractions of the spin-2 production modes. In blue for the SM and in red for the spin-2-model. The black dots are the data values. The difference between the red and blue dots corresponds to the sensitivity. The first three plots are for the three channels separately and in the last plot they are combined.*

7 Summary

For the investigation of the spin and CP nature of the Higgs-Boson three different channels were discussed and several hypotheses with spin=0, spin=1 and spin=2 were tested. For the channels $H \to \gamma\gamma$ and $H \to ZZ^* \to 4\ell$ results from ATLAS and CMS were presented whereas for the channel $H \to WW \to e\nu_e\mu\nu_\mu$ only results from ATLAS were shown. In the end all three channels were combined for the results of ATLAS. Furthermore two different production modes for a spin-2 model were investigated.

After the combination all alternative hypotheses could be rejected. In the channel $H \to \gamma\gamma$ with CMS the alternative hypothesis could not be rejected but there are results now which are more up-to-date.

For the future the investigation of CP-mixture states will be interesting and important since they would be a hint to CP-violation.

References

[1] LHC Higgs Cross Section Working Group, S. Heinemeyer, C. Mariotti, G. Passarino, and R. Tanaka (Eds.). Handbook of LHC Higgs Cross Sections: 3. Higgs Properties. *CERN-2013-004*, CERN, Geneva, 2013.

[2] Study of the spin of the Higgs-like boson in the two photon decay channel using 20.7 fb-1 of pp collisions collected at $\sqrt{s}$ = 8 TeV with the ATLAS detector. Technical Report ATLAS-CONF-2013-029, CERN, Geneva, Mar 2013.

[3] Georges Aad et al. Evidence for the spin-0 nature of the Higgs boson using ATLAS data. *Phys.Lett.*, B726:120–144, 2013.

[4] `http://atlas.physicsmasterclasses.org/de/zpath_hevents.htm`.

[5] Markus Schumacher. Lecture "Hadron Collider Physics". Summer semester 2014, Albert-Ludwigs-University of Freiburg.

[6] `https://inspirehep.net/record/1233713/plots`.

[7] Measurements of the properties of the Higgs-like boson in the two photon decay channel with the ATLAS detector using 25 fb^{-1} of proton-proton collision data. Technical Report ATLAS-CONF-2013-012, CERN, Geneva, Mar 2013.

[8] Properties of the observed Higgs-like resonance using the diphoton channel. Technical Report CMS-PAS-HIG-13-016, CERN, Geneva, 2013.

[9] Serguei Chatrchyan et al. Measurement of the properties of a Higgs boson in the four-lepton final state. *Phys.Rev.*, D89:092007, 2014.

[10] Georges Aad et al. Measurement of ZZ production in pp collisions at $\sqrt{s} = 7$ TeV and limits on anomalous ZZZ and $ZZ\gamma$ couplings with the ATLAS detector. *JHEP*, 1303:128, 2013.

[11] Serguei Chatrchyan et al. Study of the Mass and Spin-Parity of the Higgs Boson Candidate Via Its Decays to Z Boson Pairs. *Phys.Rev.Lett.*, 110:081803, 2013.

[12] Measurements of the properties of the Higgs-like boson in the four lepton decay channel with the ATLAS detector using 25 fb^{-1} of proton-proton collision data. Technical Report ATLAS-CONF-2013-013, CERN, Geneva, Mar 2013.

[13] Study of the spin properties of the Higgs-like particle in the $\boldsymbol{H \to WW^{(*)} \to e\nu\mu\nu}$ channel with 21 fb^{-1} of $\sqrt{s} = 8$ TeV data collected with the ATLAS detector. Technical Report ATLAS-CONF-2013-031, CERN, Geneva, Mar 2013.